SANDIA REPORT

SAND2012-10058
Unlimited Release
Printed November 2012

Polar Format Algorithm: Survey of Assumptions and Approximations

Cameron Musgrove

Prepared by
Sandia National Laboratories
Albuquerque, New Mexico 87185 and Livermore, California 94550

Sandia National Laboratories is a multi-program laboratory managed and operated by Sandia Corporation, a wholly owned subsidiary of Lockheed Martin Corporation, for the U.S. Department of Energy's National Nuclear Security Administration under contract DE-AC04-94AL85000.

Issued by Sandia National Laboratories, operated for the United States Department of Energy by Sandia Corporation.

Available to DOE and DOE contractors from
U.S. Department of Energy
Office of Scientific and Technical Information
P.O. Box 62
Oak Ridge, TN 37831

Telephone: (865) 576-8401
Facsimile: (865) 576-5728
E-Mail: reports@adonis.osti.gov
Online ordering: http://www.osti.gov/bridge

Available to the public from
U.S. Department of Commerce
National Technical Information Service
5285 Port Royal Rd.
Springfield, VA 22161

Telephone: (800) 553-6847
Facsimile: (703) 605-6900
E-Mail: orders@ntis.fedworld.gov
Online order: http://www.ntis.gov/help/ordermethods.asp?loc=7-4-0#online

SAND2012-10058
Unlimited Release
Printed November 2012

Polar Format Algorithm: Survey of Assumptions and Approximations

Cameron Musgrove
ISR Analysis & Applications
Sandia National Laboratories
P.O. Box 5800
Albuquerque, New Mexico 87185-MS0532

Abstract

Since the Polar Format Algorithm (PFA) was first introduced by Jack Walker 30 years ago, digital processing and Moore's law have provided the means by which to process an increasing amount of data, at finer resolutions, over a larger area, and in real-time. Inherent in the polar format algorithm are assumptions that limit the focused scene size. This report presents a development of PFA for a linear frequency modulated chirp pulsed radar utilizing stretch processing to illustrate how PFA approximations are used to form an image. Also techniques to mitigate the errors resulting from the approximations are presented from a survey of literature sources. There are many techniques that are successful at increasing the focused scene size, these include image corrections made after image formation, subaperture processing, and careful selection of processing coordinates. This report only considers methods that use the polar format algorithm.

Contents

1 Introduction

Synthetic Aperture Radar (SAR) is a method by which to synthesize a larger antenna aperture from many measurements made with a small antenna. This is desirable because resolution, particularly azimuth or cross-range resolution is proportional to the size of the antenna. A larger antenna has a smaller main beam, so it is able to distinguish between objects placed closer together. It turns out for most microwave radar wavelengths the antenna size for modest resolutions require an antenna so large that it would be bigger than most airplanes. It is much easier to mount a small antenna to an airplane, resulting in the need to synthesize a larger antenna aperture to obtain fine azimuth resolution.

Figure 1.1 shows an example of a fine resolution SAR image. Objects such as trees can readily be identified while other objects are more difficult to interpret. One can begin to see the advantage SAR imagery has over optical images when trying to image through clouds and rain. In the presence of weather the optical system is blind, however the SAR image remains unaffected because it is an active sensor and most microwave frequencies penetrate clouds and rain.

Figure 1.1: Example SAR Image

The Polar Format Algorithm (PFA) was developed to improve upon current range-Doppler processing techniques of the day to reduce image distortion and blurring by storing data according to a polar grid to coincide with the geometry used to collect the data samples. Although Walker's PFA was originally developed for turntable Inverse SAR data collection with a continuous wave linear frequency modulated (LFM) chirp analog radar, it is readily applied to airborne SAR collections for pulsed LFM chirp radars with digital receivers [1]. As technology has advanced the amount of data that can be processed in real-time, the focused scene size limits have become the limiting factor in SAR radar systems using PFA. This report will focus on PFA assumptions and approximations, and examine corrections that have been developed to increase the focused scene size. There are many sources of image distortions within practical radar systems (i.e. uncompensated platform motion, hardware performance, etc.) that will not be addressed in this report. Even though various assumptions, simplifications, and corrections affect processing efficiency, this report will not quantitatively evaluate the efficiency of a particular correction technique because it is too dependent on the particular application,

implementation and/or hardware. Within this report only image formation methods and corrections that utilize the PFA are considered.

Chapter 2 derives the polar format algorithm for a LFM chirp waveform for a digital radar receiver to establish a model of the received signal. This received signal model is used to describe the polar format algorithm and the assumptions made in its development that enable it to resolve the scatterer locations within the image. Classic image scene size limits and associated distortions are demonstrated.

While PFA does not require the scene height to be assumed flat, it is a widely used assumption. Chapter 3 describes the resulting image distortion effects in terms of height of focus and layover.

Higher order phase errors must be compensated to extend scene size beyond limits. Chapter 4 describes several techniques that have been developed to correct wavefront curvature errors. PFA assumes the radar wavefront is flat; this assumption breaks down under certain conditions. These higher order phase error terms arise from PFA's assumption the radar wavefront is flat, where it is actually curved. As will be shown later in this report, the degree of curvature varies with range, wavelength, and resolution. A simple image domain resample can correct major displacement errors, however as the image size increases, there are higher order errors that need to be corrected to maintain image focus. This chapter will present three main approaches and variations thereof that have been developed for higher order corrections, they include: space-variant post filter, polar formatted subapertures, and dual format algorithm.

Chapter 5 summarizes the assumptions made for PFA through this report. Also this chapter suggests future work directions to further expand the scene size limit for PFA.

2 Polar Format Algorithm

The polar format algorithm for synthetic aperture radar imaging was developed over 30 years ago by Jack Walker to overcome the resolution limits imposed by motion through resolution cells for the range-Doppler processing algorithms of the day [1]. The original implementation described by Walker was optically processed [1]; today in its digital implementation it is one of the most popular algorithms known for its image quality and processing efficiency.

The polar format algorithm is essentially a method by which data is collected on a polar grid at constant angle increments [2,3]. To form an image a 2D Fourier transform is applied to the data [2,3]. To properly apply the Fast-Fourier Transform algorithm in the digital domain, the data is interpolated from a polar grid to a rectangular grid before the FFT is applied to the data [2,3]. This coordinate transformation is also advantageous for most image display systems because they utilize a rectangular grid of pixels to display images. There are many variations of the PFA processing sequence and a small set of alternatives can be found in [2,3,4,5]; each variation is suited for its particular application and/or processor efficiency.

This chapter is organized into several sections. First an expression for the phase history is developed for a digital, pulsed, LFM chirp radar system. The phase history is the data that is starting point for image formation. Next, the residual video phase error term in the phase history is addressed. Then a detailed explanation is made for how the polar format algorithm is able to resolve the scatterer location. The classic scene size limits for PFA are expressed and followed by examples of the defocus effects that arise when the classic limits are exceeded.

2.1 Expression for Phase History Data

The LFM chirp waveform expression and deramp process on receive is developed in several sources [1,2,3,5,6] but is repeated here for completeness to illustrate the assumptions made in the formulation, and serve as a reference for the error corrections in later chapters. The phase history development and nomenclature in this section and succeeding sections 2.2, 2.3, and 2.4 follow [6].

Starting with an expression for the transmitted signal from a LFM chirp, pulsed radar [6]

$$X_T(t,n) = A_T rect\left(\frac{t-t_n}{T}\right)\exp j\left\{\phi_{T,n} + \omega_{T,n}(t-t_n) + \frac{\gamma_{T,n}}{2}(t-t_n)^2\right\} \quad (2.1)$$

Where:

A_T = amplitude of the transmitted pulse

t = time

n = index value of pulse number, $-N/2 \le n \le N/2$

t_n = reference time of nth pulse

T = transmitted pulse width

$\phi_{T,n}$ = transmit waveform reference phase of nth pulse

$\omega_{T,n}$ = transmit waveform reference frequency of nth pulse

$\gamma_{T,n}$ = transmit waveform chirp rate of nth pulse

The received echo from a point scatterer [6]

$$X_R(t,n) = A_R rect\left(\frac{t-t_n-t_{s,n}}{T}\right)\exp j\left\{\phi_{T,n} + \omega_{T,n}(t-t_n-t_{s,n}) + \frac{\gamma_{T,n}}{2}(t-t_n-t_{s,n})^2\right\} \quad (2.2)$$

Where

A_R = amplitude of received pulse

$t_{s,n}$ = echo delay time of the received echo for the nth pulse

By definition stretch processing mixes the received signal with a copy of the transmitted signal generated by the local oscillator [6]

$$X_L(t,n) = rect\left(\frac{t-t_n-t_{m,n}}{T_L}\right)\exp j\left\{\phi_{L,n} + \omega_{L,n}(t-t_n-t_{m,n}) + \frac{\gamma_{L,n}}{2}(t-t_n-t_{m,n})^2\right\} \quad (2.3)$$

Where

$t_{m,n}$ = reference delay time of nth LO pulse

T_L = LO pulse width

$\phi_{L,n}$ = LO waveform reference phase of nth LO pulse

$\omega_{L,n}$ = LO waveform reference frequency of nth LO pulse

$\gamma_{L,n}$ = LO waveform chirp rate of nth LO pulse

Which yields a baseband video signal [6]

$$X_V(t,n) = X_R(t,n)\,X_L^*(t,n) \tag{2.4}$$

For the magnitude of $X_V(t,n)$, the rectangle functions illustrate this is a pulsed radar system, and the magnitude of the return A_R is a function of the target RCS. The phase of $X_V(t,n)$ is of particular importance because it contains a differential time term between the scatterer and the Motion Compensation Point (MCP). The MCP is usually located at the center of the image.

$$\Phi_V(t,n) = \Phi_R(t,n) - \Phi_L(t,n) \tag{2.5}$$

Assuming the phase offset, center frequency and chirp rates are the same for receive and LO signal, $\phi_{L,n} = \phi_{T,n}$, $\omega_{L,n} = \omega_{T,n}$, $\gamma_{L,n} = \gamma_{T,n}$, the phase can be expressed as

$$\begin{aligned}\Phi_R(t,n) &= \phi_{T,n} + \omega_{T,n}\left(t - t_n - t_{s,n}\right) + \frac{\gamma_{T,n}}{2}\left(t - t_n - t_{s,n}\right)^2 \\ \Phi_L(t,n) &= \phi_{T,n} + \omega_{T,n}\left(t - t_n - t_{m,n}\right) + \frac{\gamma_{T,n}}{2}\left(t - t_n - t_{m,n}\right)^2\end{aligned} \tag{2.6}$$

Expanding all the time terms reveals many terms can be cancelled. To simplify, recognize the relations

$$\begin{aligned}\left(t - t_n - t_{m,n}\right)\left(t_{m,n} - t_{s,n}\right) &= tt_{m,n} - tt_{s,n} - t_n t_{m,n} + t_n t_{s,n} - {t_{m,n}}^2 + t_{m,n} t_{s,n} \\ {t_{s,n}}^2 &= \left(t_{m,n} - t_{s,n}\right)^2 - {t_{m,n}}^2 - 2t_{m,n} t_{s,n}\end{aligned} \tag{2.7}$$

That produces

$$\Phi_V(t,n) = \omega_{T,n}\left(t_{m,n} - t_{s,n}\right) + \frac{\gamma_{T,n}}{2}\left(2\left(t - t_n - t_{m,n}\right)\left(t_{m,n} - t_{s,n}\right) + \left(t_{m,n} - t_{s,n}\right)^2\right) \qquad (2.8)$$

Expanding the chirp term and applying the following transforms from time to range following [6]

$$\begin{aligned} t_{m,n} &= \frac{2}{c}\left|r_{c,n}\right| \\ t_{s,n} &= \frac{2}{c}\left|r_{s,n}\right| \\ \left(t - t_n - t_{m,n}\right) &= \left(iT_{s,n}\right) \text{ for } -I/2 \le i \le I/2 \end{aligned} \qquad (2.9)$$

Where

$r_{c,n}$ = position vector of the radar with respect to the scene center

$r_{s,n}$ = position vector of the radar with respect to the scatterer point

i = intra-pulse sampling index

$T_{s,n}$ = intra-pulse sampling interval

I = number of fast-time samples

Now the video phase can be described as

$$\Phi_V(t,n) = \left(\omega_{T,n} + \gamma_{T,n} iT_{s,n}\right)\left(\frac{2}{c}\right)\left(\left|r_{c,n}\right| - \left|r_{s,n}\right|\right) + \frac{2\gamma_{T,n}}{c^2}\left(\left|r_{c,n}\right| - \left|r_{s,n}\right|\right)^2 \qquad (2.10)$$

Defining the distance from the scene center to the scatterer, as measured by the radar, [6]

$$r_{cs,n} = \left|r_{c,n}\right| - \left|r_{s,n}\right| \qquad (2.11)$$

The video phase can now be expressed as

$$\Phi_V(t,n) = \left(\omega_{T,n} + \gamma_{T,n} iT_{s,n}\right)\left(\frac{2}{c}\right)\left(r_{cs,n}\right) + \frac{2\gamma_{T,n}}{c^2}\left(r_{cs,n}\right)^2 \qquad (2.12)$$

The complete expression for the video signal is

$$X_V(i,n) = A_R \exp j\left\{\left(\omega_{T,n} + \gamma_{T,n} i T_{s,n}\right)\left(\frac{2}{c}\right)\left(r_{cs,n}\right) + \frac{2\gamma_{T,n}}{c^2}\left(r_{cs,n}\right)^2\right\} \quad (2.13)$$

Equation 2.13 is an exact expression for the signal received in terms of the differential range of the scatter from the center of the scene for an LFM chirp radar. The next task is to resolve the scatterer's range and cross-range location from this expression.

2.2 Residual Video Phase Error

The second phase term in equation 2.13, $\frac{2\gamma_{T,n}}{c^2}\left(r_{cs,n}\right)^2$, is called the Residual Video Phase Error (RVPE). The original PFA [1] ignored the RVPE, though this error does vary with scene size and under certain conditions will be noticeable in imagery. This error is a direct result of the de-chirp on receive operation for a radar system using stretch processing; it is not a result of the polar format algorithm [2]. For instance, if the radar system used matched filtering instead of stretch processing, this error term would not be present in the video phase [2]. Because this is an error introduced by stretch processing, it is a system dependent error not the result of PFA. Its correction will not be covered in this report. In appendix C of [2] an analytical pre-processing method is described where the residual video phase is completely removed. Also, [6] provides a similar method to remove the residual video phase error.

2.3 Recover Scatterer Coordinates

The first phase term in equation 2.13, specifically $r_{cs,n}$, represents an indirect measurement by the radar. Radar systems can only measure time, and only within a certain precision; the radar must use an estimate of the speed of light to calculate ranges. Nonetheless, the time measured by the radar is dependent on the actual ranges and for scatterers in the same scene the speed of light can be assumed constant. Using this differential range measurement, $r_{cs,n}$, of range in each pulse it is the task of image formation to resolve a X, Y, and Z location for each scatterer to create an image of the scene. The imaging geometry for the scene is shown in Figure 2.1 below to relate the radar flight path and image coordinates.

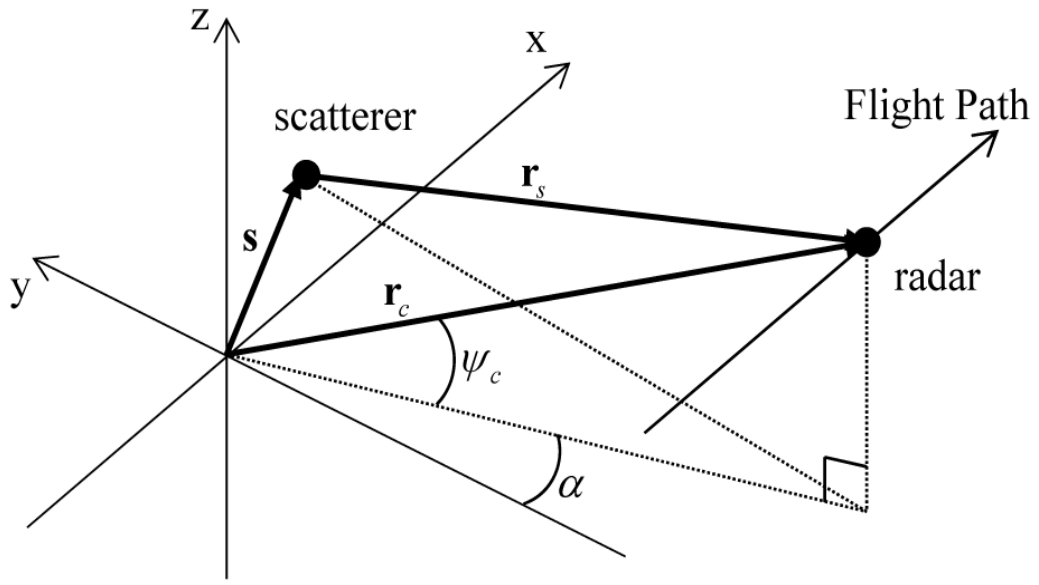

Figure 2.1: Imaging Geometry [6]

The range term $r_{cs,n}$ is a differential range between the scatterer distance to the radar, $\left|\mathbf{r}_{s,n}\right|$ and the scene center distance to radar, $\left|\mathbf{r}_{c,n}\right|$

$$r_{cs,n} = \left|\mathbf{r}_{c,n}\right| - \left|\mathbf{r}_{s,n}\right| \tag{2.14}$$

From geometry in figure 2.1, $\left|\mathbf{r}_{s,n}\right|$ can be expressed as

$$\left|\mathbf{r}_{s,n}\right| = \left|\mathbf{r}_{c,n} - \mathbf{s}\right| \tag{2.15}$$

Following the methodology in [1], the Law of Cosines can be applied to vectors such that

$$\left|\mathbf{r}_{c,n} - \mathbf{s}\right| = \sqrt{\left|\mathbf{r}_{c,n}\right|^2 + \left|\mathbf{s}\right|^2 - 2\mathbf{r}_{c,n} \bullet \mathbf{s}} \tag{2.16}$$

Rearranging to

$$\left|\mathbf{r}_{c,n}-\mathbf{s}\right|=\left|\mathbf{r}_{c,n}\right|\sqrt{1+\frac{\left|\mathbf{s}\right|^2-2\mathbf{r}_{c,n}\bullet\mathbf{s}}{\left|\mathbf{r}_{c,n}\right|^2}} \tag{2.17}$$

Generalizing the square root term to

$$\left(1+x\right)^n \tag{2.18}$$

A Taylor Series expansion of the following standard form can be applied to 2.18

$$f\left(x\right)=\sum_{i=0}^{\infty}\frac{\left(x-x_0\right)^i f^{(i)}\left(x_0\right)}{i!} \tag{2.19}$$

Expanding about the point $x_0=0$ results in this expression

$$\left(1+x\right)^n=1^n+xn1^{n-1}+\frac{1}{2}x^2n\left(n-1\right)1^{n-2}+... \tag{2.20}$$

If $n=\frac{1}{2}$ the expansion becomes

$$\sqrt{1+x}=1+\frac{1}{2}x-\frac{1}{8}x^2+... \tag{2.21}$$

Using the Taylor Series expansion 2.21 in 2.17 results in the expression

$$\left|\mathbf{r}_{c,n}-\mathbf{s}\right|=\left|\mathbf{r}_{c,n}\right|\left[1+\frac{1}{2}\left(\frac{\left|\mathbf{s}\right|^2-2\mathbf{r}_{c,n}\bullet\mathbf{s}}{\left|\mathbf{r}_{c,n}\right|^2}\right)-\frac{1}{8}\left(\frac{\left|\mathbf{s}\right|^2-2\mathbf{r}_{c,n}\bullet\mathbf{s}}{\left|\mathbf{r}_{c,n}\right|^2}\right)^2+...\right] \tag{2.22}$$

Walker [1] makes the assumption that the object (or distance from scene center $\left|\mathbf{s}\right|$) is much less than the distance of the radar from the scene center thereby eliminating the $\left|\mathbf{s}\right|^2$ term and approximates equation 2.22 as

$$\left|\mathbf{r}_{c,n}-\mathbf{s}\right|\approx\left|\mathbf{r}_{c,n}\right|\left[1-\frac{\mathbf{r}_{c,n}\bullet\mathbf{s}}{\left|\mathbf{r}_{c,n}\right|^2}\right] \tag{2.23}$$

Using a spherical to rectangular coordinate conversion with the geometry defined in figure 2.1, expressions for $\mathbf{r}_{c,n}$ and $\mathbf{s}$ are

$$\begin{aligned}\mathbf{r}_{c,n} &= \left\langle \left|\mathbf{r}_{c,n}\right| \cos\psi_{c,n} \sin\alpha_n, -\left|\mathbf{r}_{c,n}\right| \cos\psi_{c,n} \cos\alpha_n, \left|\mathbf{r}_{c,n}\right| \sin\psi_{c,n} \right\rangle \\ \mathbf{s} &= \left\langle s_x, s_y, s_z \right\rangle \end{aligned} \tag{2.24}$$

Computing the dot product as

$$\mathbf{r}_{c,n} \bullet \mathbf{s} = \left|\mathbf{r}_{c,n}\right| \left[s_x \cos\psi_{c,n} \sin\alpha_n - s_y \cos\psi_{c,n} \cos\alpha_n + s_z \sin\psi_{c,n} \right] \tag{2.25}$$

Equation 2.23 becomes

$$\left|\mathbf{r}_{c,n} - \mathbf{s}\right| \approx \left|\mathbf{r}_{c,n}\right| - \left[s_x \cos\psi_{c,n} \sin\alpha_n - s_y \cos\psi_{c,n} \cos\alpha_n + s_z \sin\psi_{c,n} \right] \tag{2.26}$$

Substituting equation 2.26 into equation 2.15 then into equation 2.14 yields

$$r_{cs,n} \approx \left[s_x \cos\psi_{c,n} \sin\alpha_n - s_y \cos\psi_{c,n} \cos\alpha_n + s_z \sin\psi_{c,n} \right] \tag{2.27}$$

This is an expression of the differential range in terms of the scatterer location from using the first two terms of the Taylor series expansion. The objective for image formation is to recover the position of $\mathbf{s}$. A flat scene can be assumed, forcing $s_z = 0$, where the implications of this assumption is discussed later in chapter 3

$$r_{cs,n} \approx s_x \cos\psi_{c,n} \sin\alpha_n - s_y \cos\psi_{c,n} \cos\alpha_n \tag{2.28}$$

Using 2.28 in the expression for the signal phase

$$X_V(i,n) \approx A_R \exp j\left\{ \left(\omega_{T,n} + \gamma_{T,n} T_{s,n} i\right) \frac{2}{c} \left(s_x \cos\psi_{c,n} \sin\alpha_n - s_y \cos\psi_{c,n} \cos\alpha_n \right) \right\} \tag{2.29}$$

The separation of $r_{cs,n}$ into s_x and s_y allows the position of the scatterer to be described by two complex sinusoids. This means that a Fourier transform can not only be used to resolve the scatterer location by the frequency of the sinusoid, but the Fourier transform can operate independently on each data dimension. Why not use more Taylor series terms in image formation? Adding more terms to the differential range introduces, effectively, more sinusoids

that are functions of both s_x and s_y; the separability is lost. Because of this approximation, the Fourier transform does not ideally resolve the location of the individual scatterers and noticeable errors are noticeable under certain conditions. The focused scene size limit is dependent on the difference between the actual differential range and the Taylor series approximation of the differential range.

2.4 Scene Size Limits

Scene size limits can be set by the amount of phase error that is deemed tolerable from neglecting terms in equation 2.22. To find the phase error, one simply needs to include more terms from the differential range expansion in the expression for video phase. Walker [1] chose the two dominant terms from the differential range expansion in equation 2.22, they are

$$\frac{\left(\mathbf{r}_{c,n} \bullet \mathbf{s}\right)^2}{2\left|\mathbf{r}_{c,n}\right|^4} - \frac{\left|\mathbf{s}\right|^2}{2\left|\mathbf{r}_{c,n}\right|^2} \tag{2.30}$$

From these terms, Walker [1] expresses them in terms of their s_x and s_y image coordinates and uses a two dimensional Taylor series expansion at the scene center to express these differential range terms in linear, quadratic, and higher order terms. The linear terms result in a shift in image coordinates, while the quadratic terms cause an astigmatic focus error and degrade resolution [1]. Since the linear terms only distort the image, they don't impact focus so Walker [1] uses the single dominant quadratic term from the Taylor series expansion of the two differential range terms to establish the focused scene diameter as

$$D \le 4\rho\sqrt{\frac{2\left|r_{c,0}\right|\phi_{qpe,\max}}{\pi\lambda_0}} \tag{2.31}$$

Where

D is the cross-range or range scene diameter

ρ is resolution

$\left|r_{c,0}\right|$ is the range from scene center to the radar at the center of the aperture

For a radar with center frequency of 16.8 GHz, figure 2.2 shows the classic scene diameter limits using equation 2.31 over a range up to 50 km with an allowable quadratic phase error of $\frac{\pi}{2}$ radians. Notice that finer resolution and shorter ranges result in smaller focused scene limits. Figure 2.3 shows the scene size limit for an UHF radar with the same allowable phase error, resolution, and range is much less than the Ku radar allowable scene size. It is up to the radar system designer to evaluate these limits with their system to determine if PFA is the best image formation choice for their system.

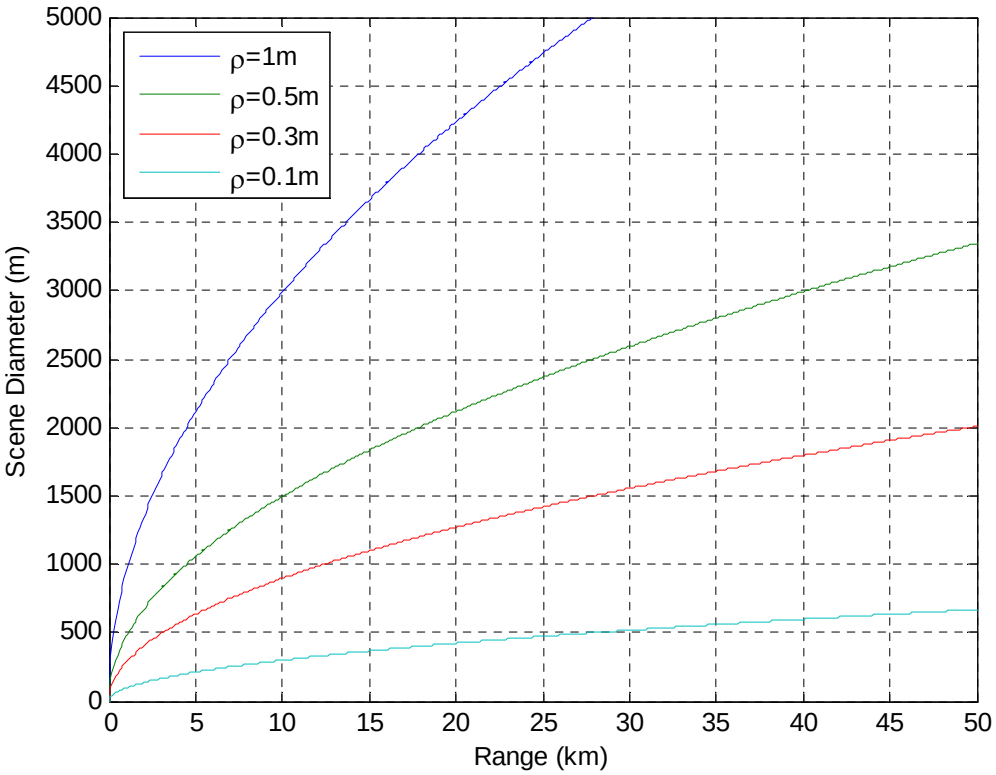

Figure 2.2: Scene Diameter Limit for Ku Radar

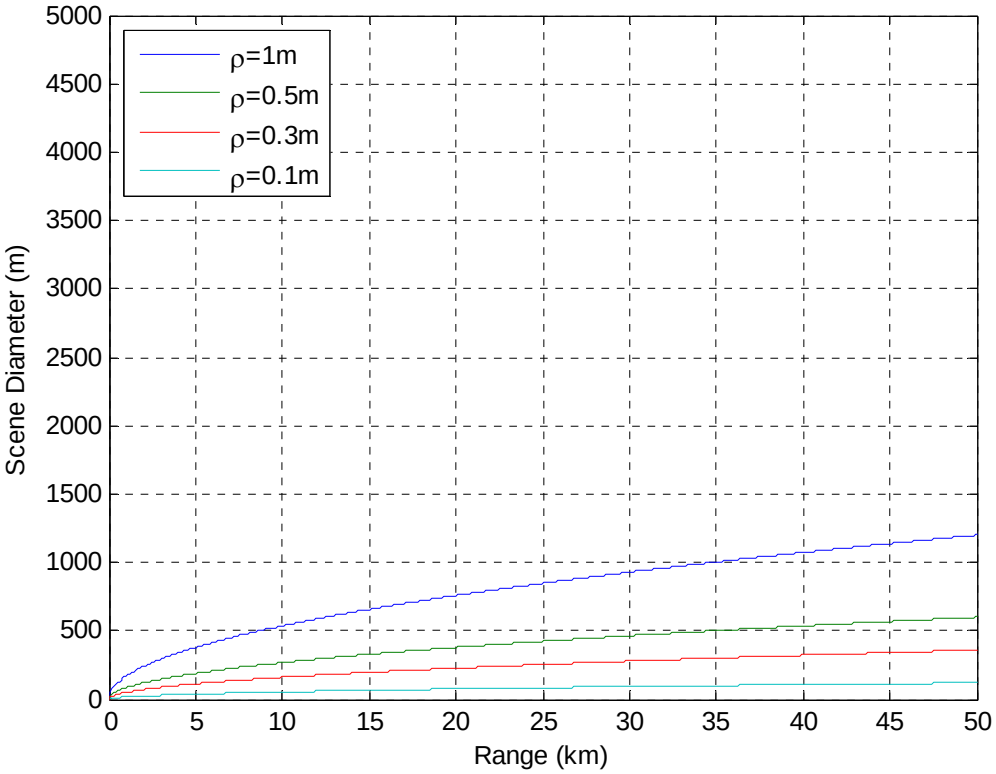

Figure 2.3: Scene Diameter Limit for UHF Radar

2.5 Image Defocus Effects

In this section, the resulting image distortions from PFA approximations will be demonstrated by simulation of point targets in a SAR scene. A Ku band radar was selected for these simulations. Figure 2.4 below shows a 100m by 100m field of point targets with 1 m resolution at a range of 5km. According to figure 2.2 a 100m scene size is well within the 2100m focus scene size limits for 1m resolution and it can be seen the point targets appear to be evenly spaced.

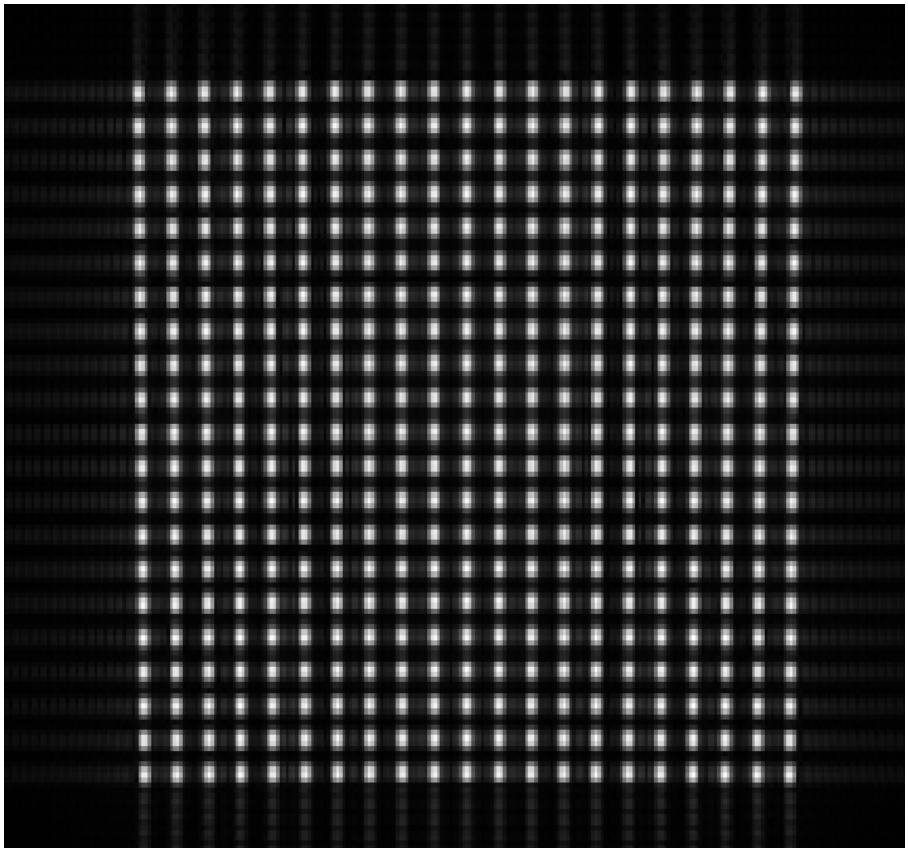

Figure 2.4: Ku Radar Small Scene Size

Here the increased scene size is not beyond the scene size limit expressed in figure 2.2; that limit is for quadratic phase errors which appear as spatially-variant defocus effects. The image shows every point target well-focused. Expanding the scene size to 850m produces figure 2.5. Despite the point target field is square and evenly spaced, the point target field in figure 2.5 appears curved. This curvature is known as geometric distortion and its correction is discussed later in section 4.1.

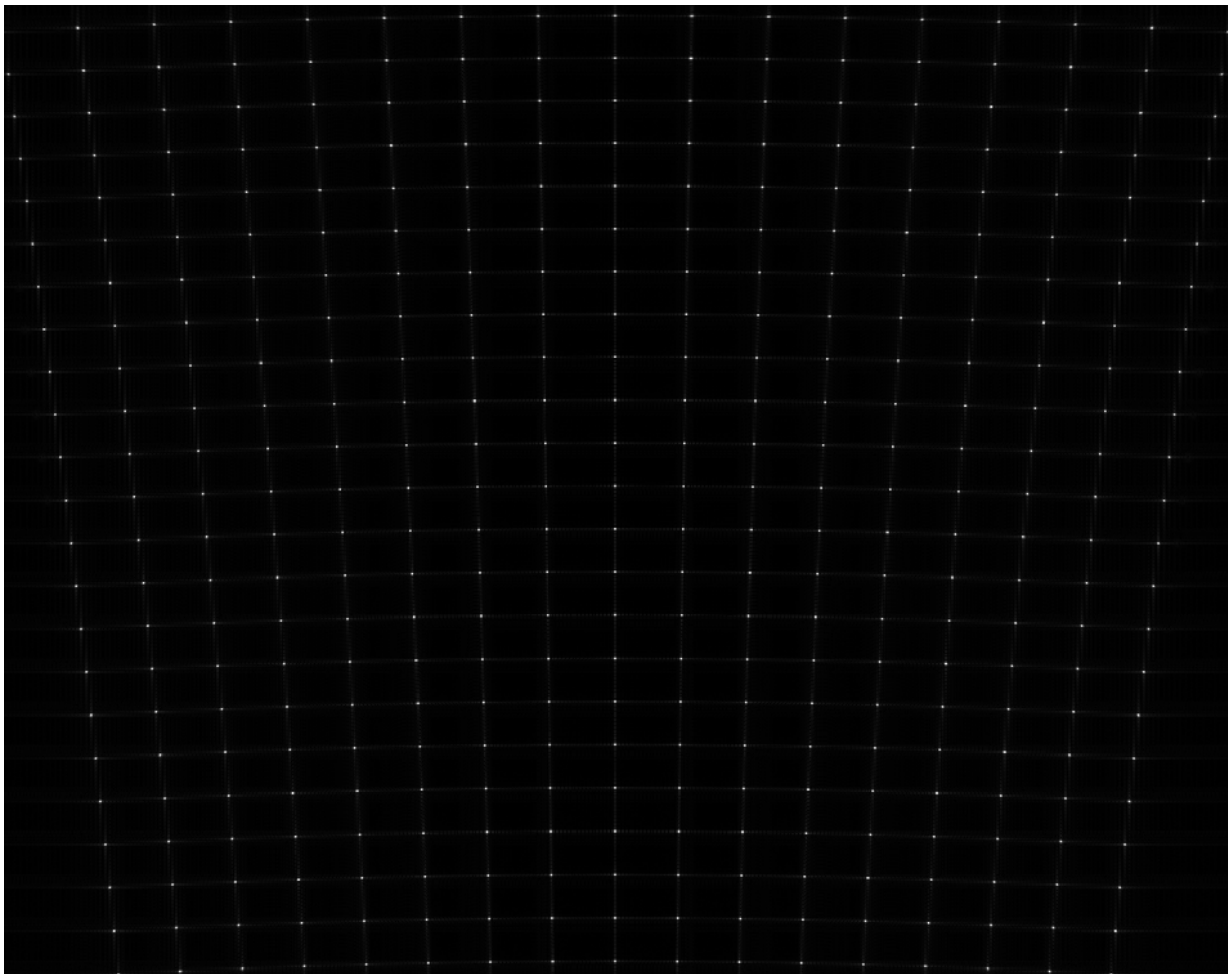

Figure 2.5: Ku Radar Large Scene Size

An example of higher order defocus effects is shown below in Figure 2.6. This scene was simulated for a Ku band radar with 0.3m resolution for a 900m swath in cross-range at a range of 5km. According to figure 2.2, the focused scene size limit for this resolution and range is 635m. Notice the point targets at the edge of the scene appear bigger and brighter than the point targets at the center; this is a result of the higher order phase errors defocusing the point targets. This distortion can be hard to notice in this report because figure 2.6 has more pixels (therefore the point targets appear smaller in this report) to cover the same overall cross-range swath as figure 2.5.

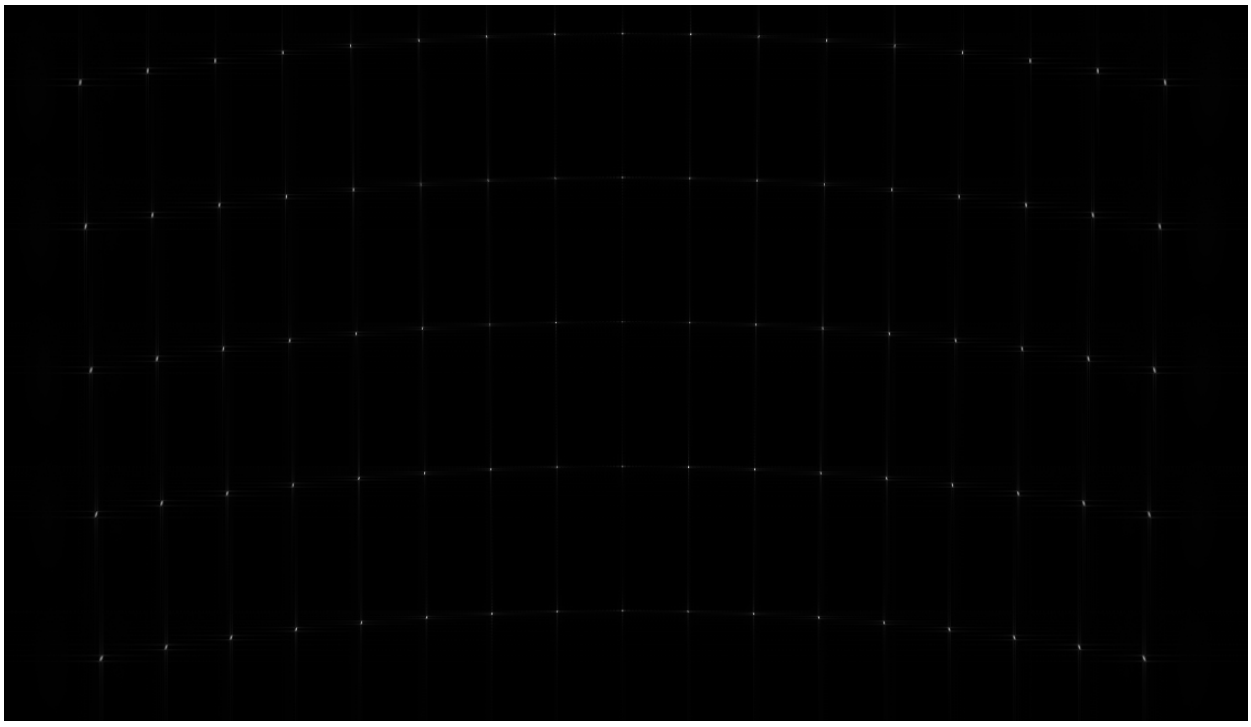

Figure 2.6: Ku Radar Large Scene and Fine Resolution

To better illustrate the defocus effects, figure 2.7 below enlarges the lower left quadrant of figure 2.6. Notice the upper-most right reflector is perfectly focused while the lowest left reflector is not only translated from its true position, it is defocused.

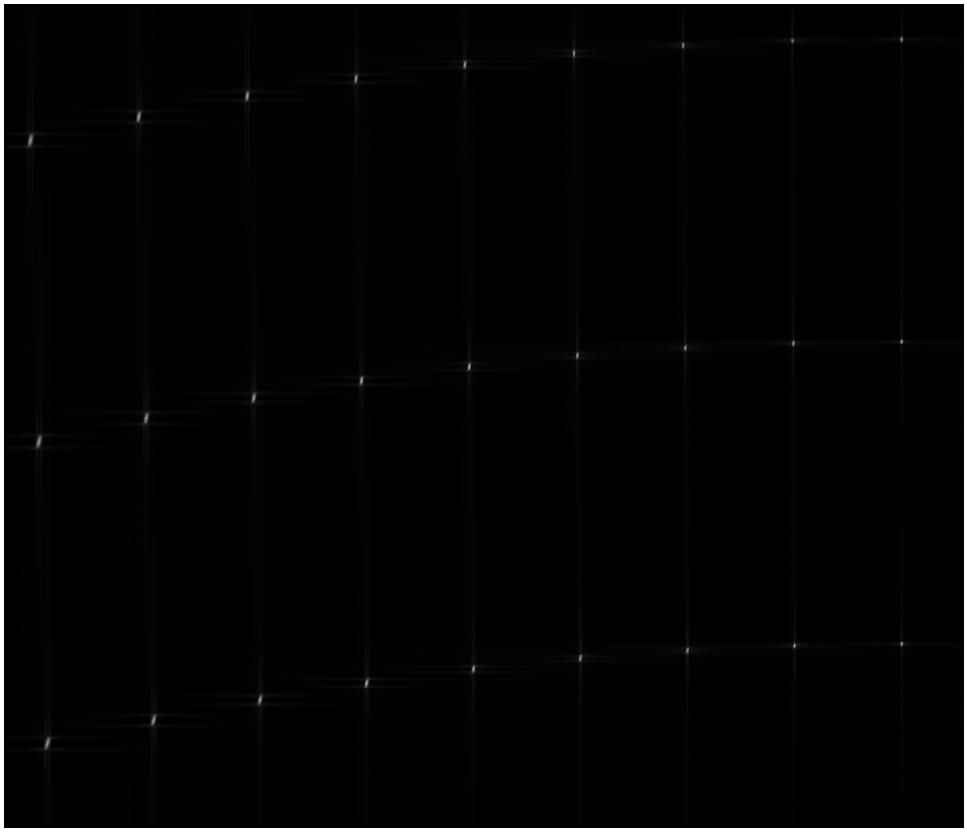

Figure 2.7: Lower Left Quadrant from Figure 2.6

2.6 Summary of PFA Approximations

PFA makes two approximations: Taylor series expansion of differential range to enable Fourier transform to resolve scatterer location, and another Taylor series expansion of the residual range term expressed as phase to establish scene size limits. These approximations simplify the mathematics such that a Fourier transform can be applied to collected data to form an image. When Walker [1] published PFA, optical image processing systems used lenses to compute Fourier transforms very efficiently. Today, the Fast-Fourier Transform algorithm makes PFA an efficient implementation for digital signal processing radars.

Over the years, radars have increased image size, decreased resolution, and decreased stand-off distance; all of which stress the simplifying assumptions inherent in PFA. Accordingly, corrections to PFA to increase the focused scene size have been developed to correct errors from using these approximations at various costs including increases in processing time and complexity. These corrections will be discussed in the remainder of this document.

3 Zero Scatterer Height Assumption

In the above development (section 2.3), the target plane (or image) was assumed to have no height. That is not the case for nearly all SAR data collections; the scene has some height. By keeping s_z in equation 2.28, equation 2.29 becomes

$$X_V(i,n) \approx A_R \exp j\left\{\left(\omega_{T,n} + \gamma_{T,n} T_{s,n} i\right)\frac{2}{c}\begin{pmatrix} s_x \cos\psi_{c,n} \sin\alpha_n \\ -s_y \cos\psi_{c,n} \cos\alpha_n \\ +s_z \sin\psi_{c.n} \end{pmatrix}\right\} \tag{3.1}$$

In this form a three-dimensional Fourier transform can resolve the scatterer location in s_x, s_y, and s_z. Further details on applying PFA in three-dimensions can be found in the literature, including [2, 3, 5].

3.1 Resolving Scatterer Height

There is a certain number and spacing of samples required in the z direction to achieve the desired height resolution. Because the number of samples in the z dimension is limited by the number of collections, many samples in z would require many data collections over the same area. For most practical radar applications this is undesirable.

There is another method to get height information from radar images. Radar systems with at least two phase centers (or with as few as two collections on the same area) can utilize a monopulse-like method to estimate the height (via angle of arrival) of the scatterers in the scene. This type of three-dimensional processing is called Interferometric SAR (IFSAR); it is not part of this report and it is explained in many sources, including [3].

3.2 Height of Focus

By assuming a flat target scene, equation 3.1 shows that if a scatterer does have height above the focus plane, an additional phase error in the data could result in undesirable image artifacts in the final image. The height limit by which scatterers above or below the focus plane are well focused is called height of focus [2]. According to [2], the height of focus is affected by out-of-plane acceleration (acceleration orthogonal to the slant plane). Significant out-of-plane motion

will decrease the height of focus in the final image. Carrara [2] provides the following expression to quantify the height of focus for a particular motion described as a 'vertical pop-up maneuver' as

$$Z_{hof} = \left(\frac{V_{xa}^2 \sin^3 \theta_c \cos \psi_c}{R_{ac} a_{zo}} \right) \left(\frac{4\rho_a^2}{\lambda_c K_a^2} \right) \tag{3.2}$$

Where

V_{xa} is the velocity component in the x direction (direction of travel)

θ_c is the squint angle at the center of the aperture

ψ_c is the grazing angle at the center of the aperture

R_{ac} is the range from the center of the scene to the Antenna Phase Center at the center of the aperture

a_{zo} is the out of slant plane acceleration

ρ_a is the azimuth resolution

λ_c is the radar wavelength at the center frequency

K_a is the azimuth broadening factor from using a window function to control sidelobes

Equation 3.2 shows that height of focus increases with coarser resolution, increasing velocity in x direction, squinting closer to broadside, and smaller grazing angle. It can be seen there is an inverse relationship between out-of-plane acceleration, a_{zo}, and height of focus. Throughout a single aperture the most dominant term is going to be out-of-plane acceleration, a_{zo}. The out-of-plane acceleration is primarily a function of the platform motion; it can be due to erratic motions induced by weather or the pilot.

A technique described in [15] has been developed for satellite implementation of PFA for very large scene sizes (>1 million square kilometers) to account for the fact that the surface of the Earth curves away from PFA's flat plane at large distances from the scene center (if the target plane is at the scene center point elevation). The image is sub-divided into regions where a

single target plane height results in tolerable height of focus errors. This process is conceptually similar to other wavefront curvature correction techniques discussed later in that it subdivides the data into regions where PFA works well.

3.3 Layover

As a consequence of the flat target plane assumption, objects with height are flattened in the imagery; this type of distortion is called layover. Layover occurs in a SAR image where the top of a tall object (i.e. a building) is at a closer range than the base of the object. In effect, the top of the object lays over the ground in front of it. Figure 3.1 shows a ray diagram illustrating layover of a building. The red arcs represent constant range contours. The reflected energy from scatterers along the same range contour will combine together and be indistinguishable from each other.

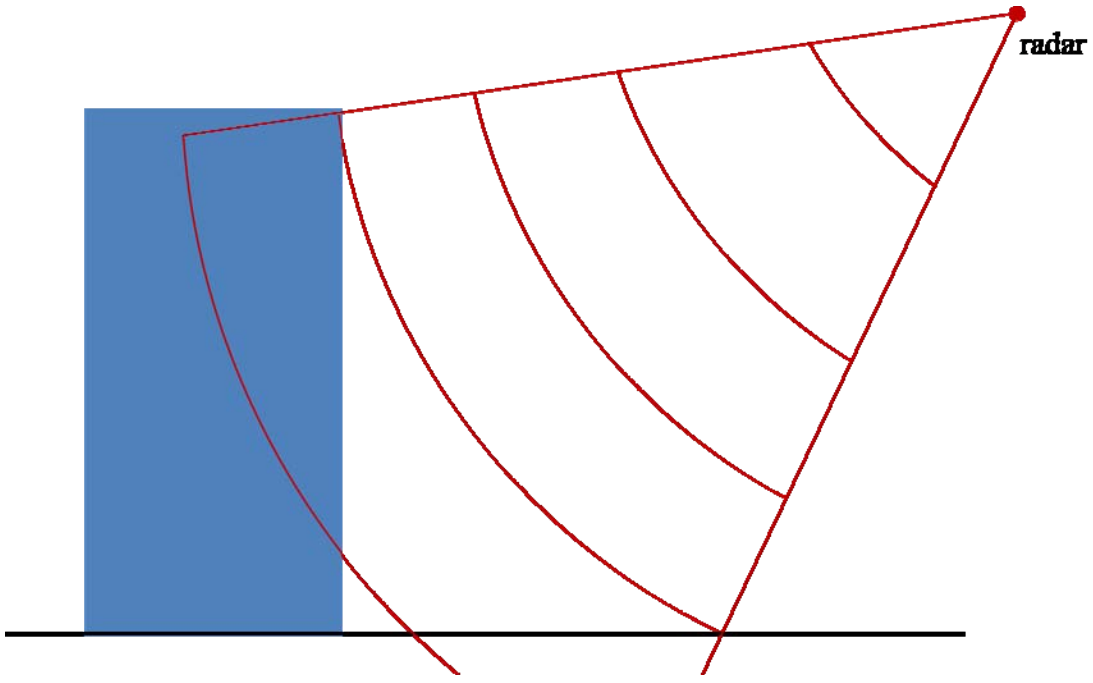

Figure 3.1: Illustration of Layover

Figure 3.1 above shows that the top of the building is at the same range contour as the ground in front of the building, therefore the energy from the scatterers at the top of building (and the face of the building) are going to add to the scatterer energy from the ground. An excellent example of layover in a SAR image can be seen below in figure 3.2. The side of the building can be seen extending out from the base of the building.

Figure 3.2: Example of Layover in SAR Image

Another interesting effect of layover is that the direction of layover is orthogonal to the flight line. For broadside collections (where the radar is looking directly left or right to the direction of travel) the layover is toward the radar. However, for squinted collections (where the radar is looking forward or back of the broadside direction) objects will lay over in a different direction

than the radar, in the direction orthogonal to the flight line. How this layover manifests itself in the imagery is not just shifting the top of the object to the left or right; depending on the object and flight trajectory, an image could show a bend in a road when actually the road is straight, or vice versa. An example of this can be found in [3] on page 86.

3.4 Summary

Although the assumption of zero scatterer height is made in PFA developed by Walker [1], there is not any part of PFA that precludes scatterer height from being used. Often it is operational and practical considerations that are eased by setting the height to zero. One practical reason to make a 2D image is that today's (and historically) image display technology is well-suited for displaying 2D images; this may change in the future with the proliferation of 3D viewing technologies. Although, if a radar could collect a sufficient amount of data in the z direction within a single pass, the height of focus would still be limited by the platform's amount of out-of-plane acceleration.

For most applications, IFSAR techniques are preferable to 3D Fourier transforms because they tend to require less data collections (i.e. fly-bys) of the same scene. However, each application and radar system is unique and there is a trade-space of techniques that are best suited to meet the end-user's needs.

4 Wavefront Curvature Correction

One of the simplifications made in PFA is the truncation of Taylor series expansion terms, expressing the range from scene center to each scatterer ($r_{cs,n}$ from equation 2.14). The first two terms of the Taylor series expansion allow a Fourier transform to convert the frequency domain data into spatial domain data, however the truncated terms do contribute additional phase errors that appear as undesirable artifacts in the imagery under certain conditions. In practice, scene sizes are limited by a certain amount of phase error such that resulting image artifacts are not noticeable in the image [1, 3].

The truncation of Taylor series expansion terms to the first two terms effectively assumes the wavefront is flat, when actually the wavefront has curvature to a degree that depends on several factors. Wavefront curvature is the curvature of the phase front of the transmitted wave from the radar as the transmitted wave propagates through space; it is least apparent when range >> scene size. As radars get closer in range and finer azimuth resolution, the wavefront is more curved and the neglected terms produce noticeable image distortions. When viewing the final radar image, wavefront curvature can be expressed in three categories of Taylor series expansion terms: linear, quadratic, and higher order. Linear terms cause straight objects appear curved [2, 7]. This is also called a geometric distortion and the correction can be a simple interpolation operation on the final image product that is discussed in section 4.1. The quadratic term defocuses the image by an amount that varies with each scatterer's location in the image (it is not constant with range and said to be spatially-variant) [7]. Higher order terms defocus the entire image [7].

The quadratic term has been the limiting factor of the focused scene size limit in PFA [1]. There have been a few distinct methods proposed to correct the quadratic wavefront curvature errors with PFA: Space-Variant Post-Filter, polar formatted subapertures, and dual format algorithm. Most methods for wavefront curvature are variations upon the Space-Variant Post Filter by Doren (section 4.2) adapted for a different flight geometry and/or radar application.

All of these methods seek to reduce or minimize the residual range error for data collected on a polar grid while using the Fourier transform. There are literally infinite ways to implement these corrections given the differences in radars, flight platforms, and processing hardware. In section

4.2 an inefficient matched filter implementation becomes efficient in section 4.2.3 by changing the flight geometry, application, and technology advances over 12 years.

A survey of the existing methods to compensate for wavefront curvature distortions is presented in the succeeding sections of this chapter. First, corrections for the geometric distortion from the linear terms of the Taylor series expansion are discussed; these corrections are well understood and utilized by nearly all implementations of PFA and its derivatives. Then Doren's Space-Variant Post Filter is presented followed by variations thereof in succeeding subsections. Section 4.3 discusses a different approach to wavefront curvature correction by polar formatted subapertures. Finally, section 4.4 describes a unique approach called dual format algorithm.

4.1 Geometric Distortion from Range Curvature

After forming the image with PFA, depending on the radar system parameters, a geometric distortion could be noticeable within the image. A geometric distortion is noticeable when a straight object, such as a road, appears curved within the image, and vice-versa, depending on the curvature of the object relative to the radar.

An image domain resampling process is all that is needed to remove the effects of this geometric distortion. Carrara [2] gives details and the transformation equations to implement the resampling process. It is a mapping from the apparent location of a scatterer in the image to the scatterer's true location within the image. This location difference arises from the fact PFA collects the fast and slow-time data on a polar grid in the frequency domain. To use the FFT, the polar grid points (data samples) are interpolated to a regularly spaced grid. At this point the data for the entire image does not change its values, only there are new sample locations. The left image in figure 4.1 shows a polar arrangement of samples super-imposed on the constant range lines for a scene in a polar arrangement. The right image in figure 4.1 shows the resampled locations as being an evenly spaced rectangular grid, however the underlying data values are still curved. Therefore, a constant range line is still curved across the aperture according to the wavefront curvature for that collection geometry.

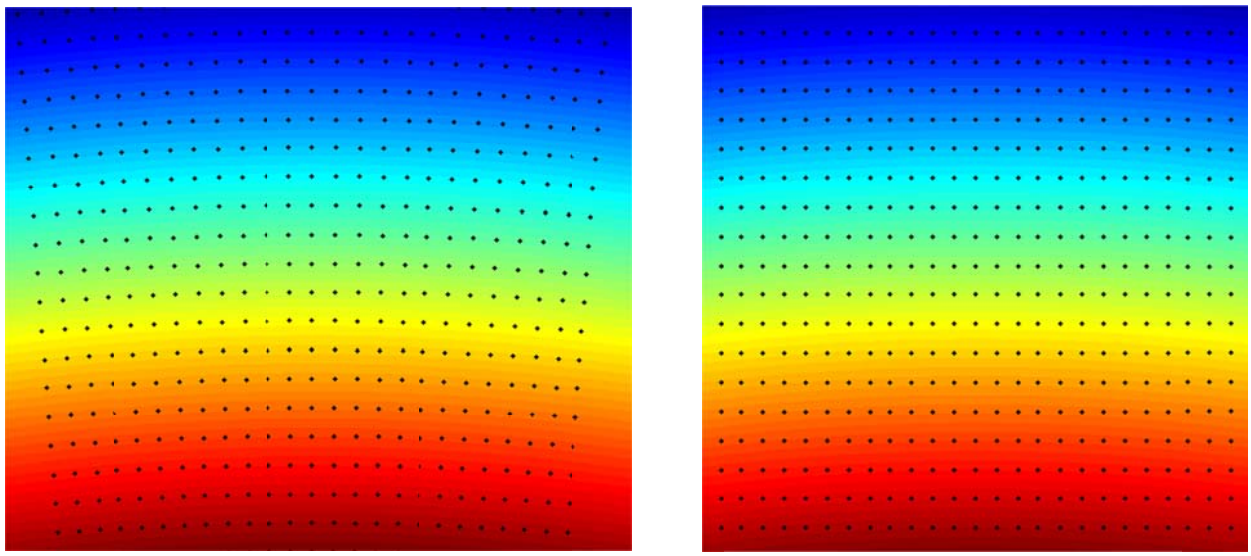

Figure 4.1: Geometric Distortion and Samples

Figure 4.2 shows a SAR image where geometric distortion is present. The long dark object running horizontal in the image is actually straight; however it appears curved in this image. Figure 4.3 shows the image after geometric distortions are corrected; the long dark object is straight.

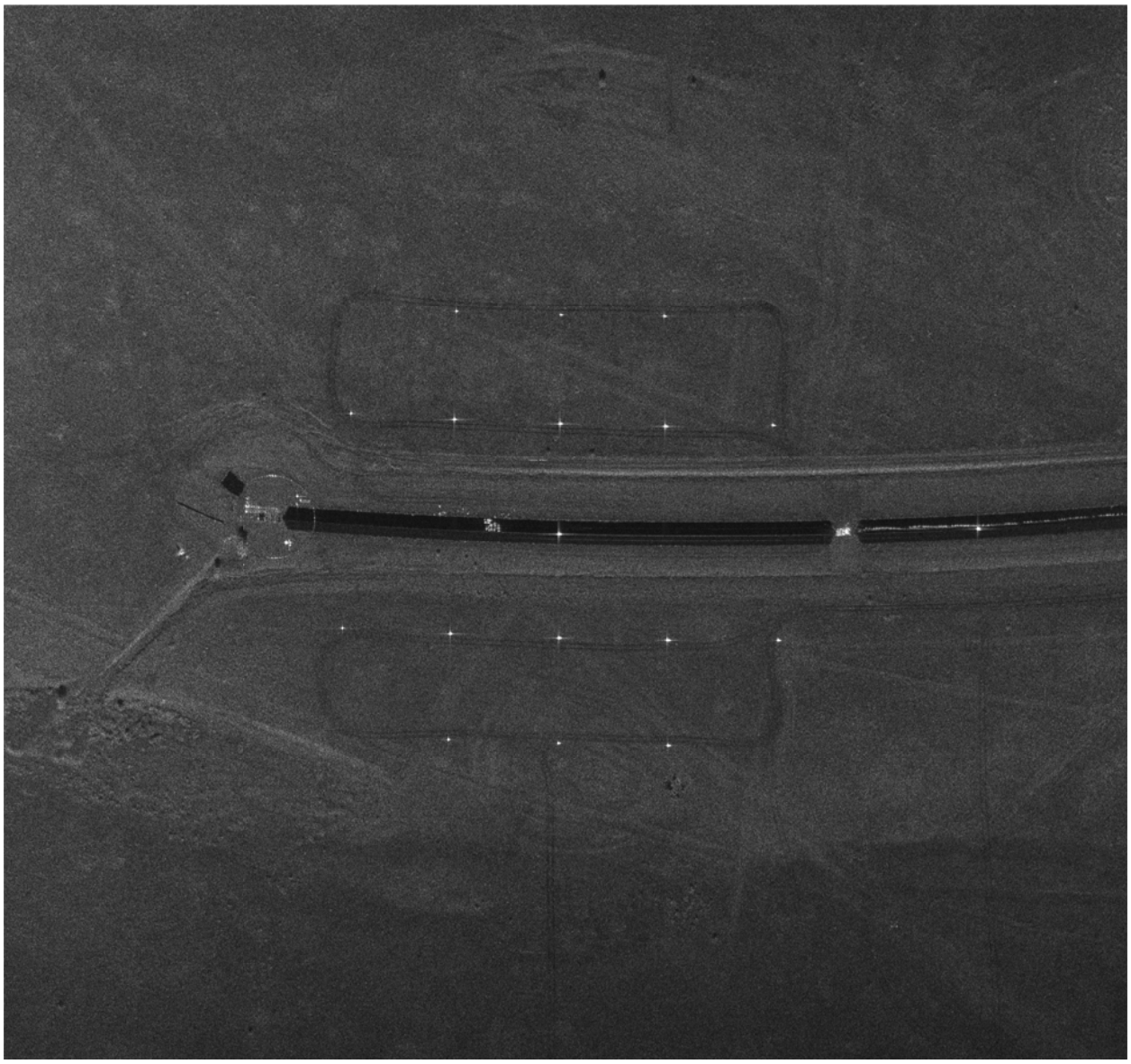

Figure 4.2: Image with Geometric Distortion

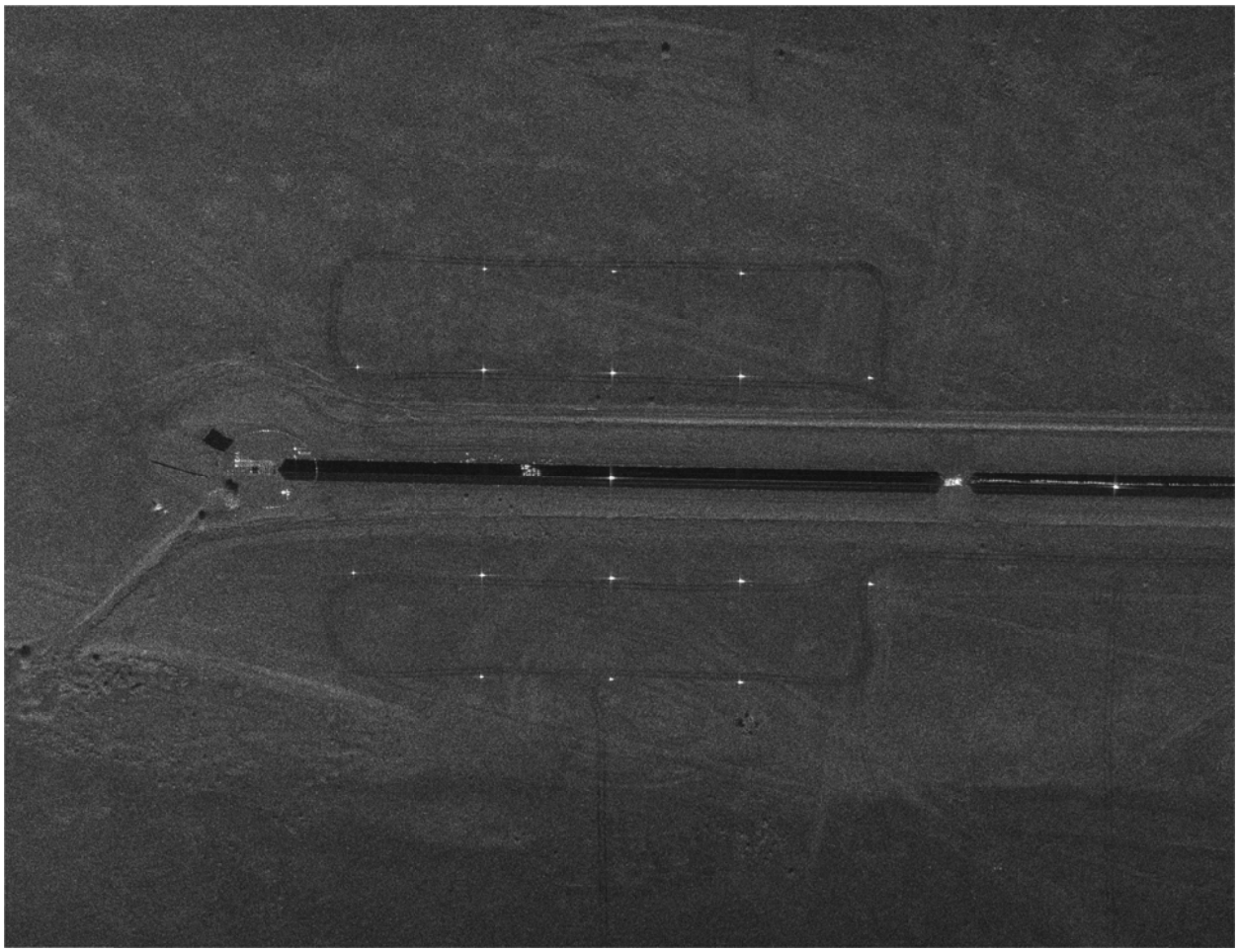

Figure 4.3: Image with Geometric Distortion Corrected

4.2 Space-Variant Post-Filter for Linear Flight Path

Doren's dissertation [7] describes a method to remove spatially variant wavefront curvature errors from imagery for a straight radar flight path. The spatially variant (or quadratic terms of the differential range) wavefront curvature error is the dominant error in PFA that limits the focused scene size. Doren calls the correction process a Space-Variant Post Filter (SVPF) because it corrects spatially varying errors (errors that vary with position in the scene) and it is applied after image formation on the complex image [7]. By identifying additional terms in the Taylor series expansion of the differential range, Doren corrects phase errors that contribute to wavefront curvature. The details of how Doren identifies and uses these additional Taylor series terms are summarized below.

From the expression for the demodulated, sampled video signal of a flat target scene and considering the RVPE term has been neglected or corrected (similar to equation 2.13)

$$\Phi_V(i,n) = \frac{2}{c}\left(\omega_{T,n} + \gamma_{T,n} T_{s,n} i\right)\left(\left|\mathrm{r}_{c,n}\right| - \left|\mathrm{r}_{s,n}\right|\right) \tag{4.1}$$

The above expression indicates the sampled video phase for a particular intra-pulse index i and pulse index n. From assuming a linear (or straight) flight path, Doren is able to create an expression of the Fourier domain phase history in terms of the scatter location $\left(s_x, s_y\right)$ expressed as the following range terms consistent with geometry defined in figure 2.1 [7].

$$\begin{aligned} \left|\mathbf{r}_c\right| &= \left|\mathbf{r}_{c,0}\right| \sqrt{1 + \left(\frac{X}{Y}\right)^2} \\ \left|\mathbf{r}_s\right| &= \sqrt{\left|\mathbf{r}_c\right|^2 + \left|\mathbf{s}\right|^2 - 2\left|\mathbf{r}_c\right|\left|\mathbf{s}\right| \sin\left(\arctan\left(\frac{X}{Y}\right) + \alpha_s\right)} \end{aligned} \tag{4.2}$$

Where

$\left|\mathbf{r}_{c,0}\right|$ = the range from the scene center to the center of the aperture.

X and Y are the frequency domain phase history coordinates

The scatter location is expressed as

$$\begin{aligned} s_x &= \left|\mathbf{s}\right| \cos\alpha_s \\ s_y &= \left|\mathbf{s}\right| \sin\alpha_s \end{aligned} \tag{4.3}$$

Doren expands the phase expression about the origin of the frequency domain with a Taylor series of the form

$$\begin{aligned} \Phi_{s_x,s_y}\left(k_x, k_y\right) &= a_{00} + a_{10}k_x + a_{01}k_y + a_{20}{k_x}^2 + a_{11}k_x k_y + a_{02}{k_y}^2 + \ldots \\ a_{ij} &= \left(\frac{1}{i!\,j!}\right)\left(\frac{\partial^{i+j}}{\partial {k_x}^i \partial {k_y}^j}\Phi_{s_x,s_y}\left(k_x, k_y\right)\right) \end{aligned} \tag{4.4}$$

This process is similar to the Taylor expansion used by [1] in that it is the phase expression that is approximated with the Taylor expansion. Doren's approach is different in that he considers

the full phase expression whereas Walker had only used the dominant terms for expansion (see equation 2.30). The straight flight path data collection scenario creates a straight-forward coordinate transformation between the scatter location in the image and the phase history domain. Why use the coordinate transformation? By using the coordinate transformation, Doren is calculating the frequency domain correction vector based on the scatterer location in the image. The location of the scatter in the image is used, to calculate the amount of quadratic phase error expected for that particular location. Without the image location of the scatterer the phase correction could not be calculated. Given there are other phase errors in the data from a multitude of sources, including platform position errors, the Taylor series expansion allows the calculation of the proper amount of correction only due to the quadratic term.

In [7], Doren is able to construct a correction vector that accounts for the uncompensated geometric distortion while correcting the spatially-variant errors. First the image is subdivided into regions called chips. For each chip, the correction vector is the complex conjugate of the calculated quadratic and linear phase at the center point of an image chip [7]. The correction vector is efficiently applied as a multiply operation in the frequency domain after applying a FFT to the image chip. Then an Inverse FFT operation is applied to obtain the corrected chip. The corrected chips are stitched together until processing on the whole image is complete. The size of the chip selected from the image is such that the residual phase error is tolerable, and depends on parameters for a particular radar system and application; details to select chip size can be found in [7].

Doren's method can be applied to correct for more phase errors by including more terms of the Taylor series expansion in the correction vector calculation. By correcting for the wavefront curvature, the scene size limits can increase by the amount of correction (or number of terms from Taylor expansion) applied. Doren's method is limited to use by systems that collect data along a straight line, however we will later see others have applied this technique, with some modifications, for non-linear flight geometries.

4.2.1 Wavefront Curvature for Arbitrary Flight Paths

Doerry [6] describes a method to correct for wavefront curvature for arbitrary flight paths including circle, straight line, and squinted straight line. The particular correction expressions

are dependent on the specific flight geometry, and they are applied to the image product in a similar method to Doren's SVPF by subdividing the image into chips and applying the correction in the frequency domain via FFT and IFFT operations [6].

Doerry takes a unique approach in starting with data that has completed the range interpolation operation. Range interpolation can be accomplished by a direct data interpolation after data is collected, or it could be implemented in real-time as the radar collects the data [6]. After the range dimension is resampled the spacing between azimuth samples is constant in $\tan\alpha_n$ [6]. Where α_n is the angle at the scene center between the sample location and the center of the synthetic aperture. Doerry constructs an expression of the video phase after the range interpolation from the expression for video signal (equation 2.29 above)

$$\begin{aligned} X_V(i,n) &\approx A_R \exp j\left\{\frac{2}{c}\left(\omega_{T,n}+\gamma_{T,n}T_{s,n}i\right)\left(s_x\cos\psi_{c,n}\sin\alpha_n - s_y\cos\psi_{c,n}\cos\alpha_n\right)\right\} \\ X_V(i,n) &\approx A_R \exp j\left\{\frac{2}{c}\left(\omega_0+\gamma_0 T_{s,0}i\right)\kappa_n\left(s_x\cos\psi_{c,n}\sin\alpha_n - s_y\cos\psi_{c,n}\cos\alpha_n\right)\right\} \end{aligned} \quad (4.5)$$

Real-time motion compensation can be applied by compensating the center frequency and chirp rate by [6]

$$\kappa_n = \frac{\cos\psi_{c,0}}{\cos\psi_{c,n}\cos\alpha_n} \quad (4.6)$$

Resulting in the following video expression with real-time motion compensation applied, and the first few terms of the Taylor series expansion and additional terms are shown as $\phi_{pe,n}$

$$X_V(i,n) = A_R \exp j\left\{\frac{2}{c}\left(\omega_0+\gamma_0 T_{s,0}i\right)\cos\psi_{c,0}\left(s_x\tan\alpha_n - s_y\right)+\phi_{pe,n}\right\} \quad (4.7)$$

Where $\phi_{pe,n}$ is approximated as

$$\phi_{pe,n} \approx \frac{2}{c}\left(\omega_0+\gamma_0 T_{s,0}i\right)\frac{\cos\psi_{c,0}}{\cos\psi_{c,n}\cos\alpha_n}\left[\frac{\left(\mathbf{r}_{c,n}\bullet\mathbf{s}\right)^2}{2\left|\mathbf{r}_{c,n}\right|^2}-\frac{\left|\mathbf{s}\right|^2}{2\left|\mathbf{r}_{c,n}\right|^2}\right] \quad (4.8)$$

It should be noted that these are the same phase terms that Walker used to develop focused scene size limits via two-dimensional Taylor series expansion [1]. Doerry recognized that the motion compensated phase history can be expressed as a function of $\tan\alpha_n$ [6]

$$\phi_{pe,n} \approx \left(\frac{\omega_0 + \gamma_0 T_{s,0} i}{c} \right) \cos\psi_{c,0} \left[\frac{\left(\begin{array}{l} s_y{}^2(\cos^2\psi_{c,n} - 1) - s_x{}^2 \\ -2 s_y s_x \cos^2\psi_{c,n} \tan\alpha_n \\ +\left(s_x{}^2 \cos^2\psi_{c,n} - s_x{}^2 - s_y{}^2 \right) \tan^2\alpha_n \end{array} \right)}{\left| \mathbf{r}_{c,n} \right| \cos\psi_{c,n} \sqrt{1 + \tan^2\alpha_n}} \right] \tag{4.9}$$

From the above equation, Doerry shows that same scene limits established by Walker hold for a circular flight path [6]. Furthermore, Doerry shows the focused scene limits have a dependence on grazing angle [6]. The correction expression comes from recognizing the phase expression above in equation 4.9 can be expressed as a Taylor series expansion of the phase as a function of $\tan\alpha_n$ [6]

$$\varphi\left(\tan\alpha_n\right) = \frac{\left(\begin{array}{l} s_y{}^2(\cos^2\psi_{c,n} - 1) - s_x{}^2 \\ -2 s_y s_x \cos^2\psi_{c,n} \tan\alpha_n \\ +\left(s_x{}^2 \cos^2\psi_{c,n} - s_x{}^2 - s_y{}^2 \right) \tan^2\alpha_n \end{array} \right)}{\left| \mathbf{r}_{c,n} \right| \cos\psi_{c,n} \sqrt{1 + \tan^2\alpha_n}} \tag{4.10}$$

The Taylor series expansion (equation 2.19) using phase function from 4.10 above results in [6]

$$\phi_{pe,n} \approx \left(\frac{\omega_0 + \gamma_0 T_{s,0} i}{c} \right) \cos\psi_{c,0} \left[\varphi(0) + \frac{d\varphi(0)}{d\tan\alpha_n} \tan\alpha_n + \left(\frac{1}{2} \right) \frac{d^2\varphi(0)}{d\tan^2\alpha_n} \tan^2\alpha_n + \ldots \right] \tag{4.11}$$

Doerry goes on to identify the terms of the expansion as contributing to defocusing, azimuth shift, and range shift [6]. The nice thing about this approach is that you can increase your corrections by adding additional terms from the Taylor series expansion, and the complexity scales with increased multiplies; the image has already been chipped and the FFT/IFFT applied. Another nice result of this approach, when compared to Doren's, is the linear wavefront

curvature terms are corrected at the same time as the other terms, so the phase correction terms do not have to account for the position shift from geometric correction that is done later in the image processing chain.

Doerry's SAND Report details the technique [6], while a paper from Linnehan [8] implements this wavefront correction technique for real SAR data.

4.2.2 Spatially Variant Post-Filter for Image Formed in Ground Plane

For an application where repeated collections are made for Interferometric SAR (IFSAR) processing, Preiss describes a modification to the spatially variant post-filter for when the image is formed on the ground plane, not the slant plane [16]. Preiss recomputes the Taylor series expansion of the residual phase error for ground plane geometry and in the process identifies an additional range dependent term that the slant plane formulation does not include [16]. With this additional term, and the straight flight path trajectory, Doren's SVPF can be modified to successfully apply corrections. SAR imagery is shown to demonstrate improvement from using the modified SVPF over standard PFA processing [16].

4.2.3 Polar Formatting with Spatially Variant Post-Filtering

This technique by Garber and Hawley [9] extends Doren's work [7] by correcting for wavefront curvature for circular flight geometries, and it also combines height data to correct the defocus due to terrain height differences in the image. The specific application of wide-area persistent surveillance in [9] results in many implementation details that diverge from [6,7]. These include circular flight path, rotation of images to the same orientation, and incorporating height data to improve focus for out of plane scatterers [9]. Height data could be available from the sensor though parallel processing methods, or it could be provided prior to radar data collection [9].

Fundamentally [9] is using a Taylor series expansion of the differential range to create phase error correction terms, similar to [6,7]. However, Garber uses the complete expression for the differential range phase expansion, rather than expanding the dominant terms as done in [1, 6, 7].

Garber's technique, unlike [6, 7], uses a matched filter in the image domain to apply the wavefront curvature correction for every pixel in the image. For the persistent surveillance application, the final image rotation, curvature correction, and layover correction (when height

data is available) can all be combined into one resampling step for computational efficiency [9]. It is interesting to note that Doren and others split the image into chips and avoided the matched filter operation on every pixel for computational efficiency [6, 7].

4.2.4 Space-Variant Post Filter Modified to Use Complete Range Expression

A paper by Mao, et al, [10] extends Doren's Spatially-Variant Post Filter (SVPF) to correct the complete residual range phase error. Mao is able to calculate the complete differential range $r_{cs,n}$ by knowing the position of the radar at each pulse [10]; whereas Doren assumed a linear flight path [7].

First, the image is subdivided into chips, like Doren's SVPF, such that a constant phase correction can be applied across the entire chip from using the center coordinate location such the phase error at the chip edges are within some allowable amount of phase error [10]. Next, the wavefront curvature phase error is calculated from the radar position and the location of the center of the chip [10]. Since radar position is known in the slow-time (pulse-to-pulse) coinciding with the data collection geometry, the resulting phase error corrections are defined on a polar grid. This polar grid is interpolated into a rectangular grid so the conjugate of the phase can be directly applied to the frequency domain chip [10]. All chips are processed and mosaicked together to produce a final image product [10].

This technique works well only if you have a certain amount of precision for the radar's actual position at each pulse. Any position errors will either reduce the amount of correction needed or introduce errors and artifacts into the imagery. The author [10] acknowledges this method's dependence on motion precision, but does not quantify the level required. This is not a fault as the required location/motion precision would be directly related to the allowable phase error in imagery.

Also, the author did not specifically discuss the overall performance impact from using an additional interpolation step beyond Doren's SVPF. Interpolations can be fast, but they can introduce errors, too. Doren has studied the overall performance impacts of his SVPF to maximize efficiency, so there may be a performance efficiency increase by using only a few terms of the differential range expansion.

4.2.5 Wavefront Curvature for Bistatic SAR

In papers by Wang and Zhu [17, 18] they develop a Taylor series expansion of the differential range phase for bistatic radar geometry. The bistatic development follows Doren's SVPF [7] algorithm through constructing the phase corrections and implementing the corrections on the image via chips [17]. Through simulated data it is shown that wavefront curvature corrections can be applied for bistatic case [17].

Wang and Zhu [17] also formulate scene size limit expressions using the two cubic range-only dependent phase error terms from the Taylor series expansion of the differential range phase error. Other sources, including Doren, have not attempted to quantify additional scene size limits from the remaining phase terms. It remains to be shown that these new scene size limits apply.

4.3 Polar Formatted Subapertures

Doerry, in addition to the technique described in section 4.2.1, developed another technique to expand the focused scene size limit imposed by the planar wavefront assumption in PFA. Expanding upon a previous technique employing subaperture processing in [11], Doerry describes a method to utilize multiple subapertures of subapertures, or tiers, to increase focused scene size limits [12]. Doerry's technique is part of this report because it does use polar format processing on the subapertures to form the image, while the technique in [11] is very similar, it does not use polar format processing.

The subaperture technique, as described by [12] divides the phase history data into smaller sets of data called subapertures, each subaperture overlaps (includes data values) with adjacent subapertures; Figure 4.4 illustrates this concept. The amount of overlap and size of the subaperture is determined by system parameters to limit scatterer migration (or range walk) to within a tolerable amount [11].

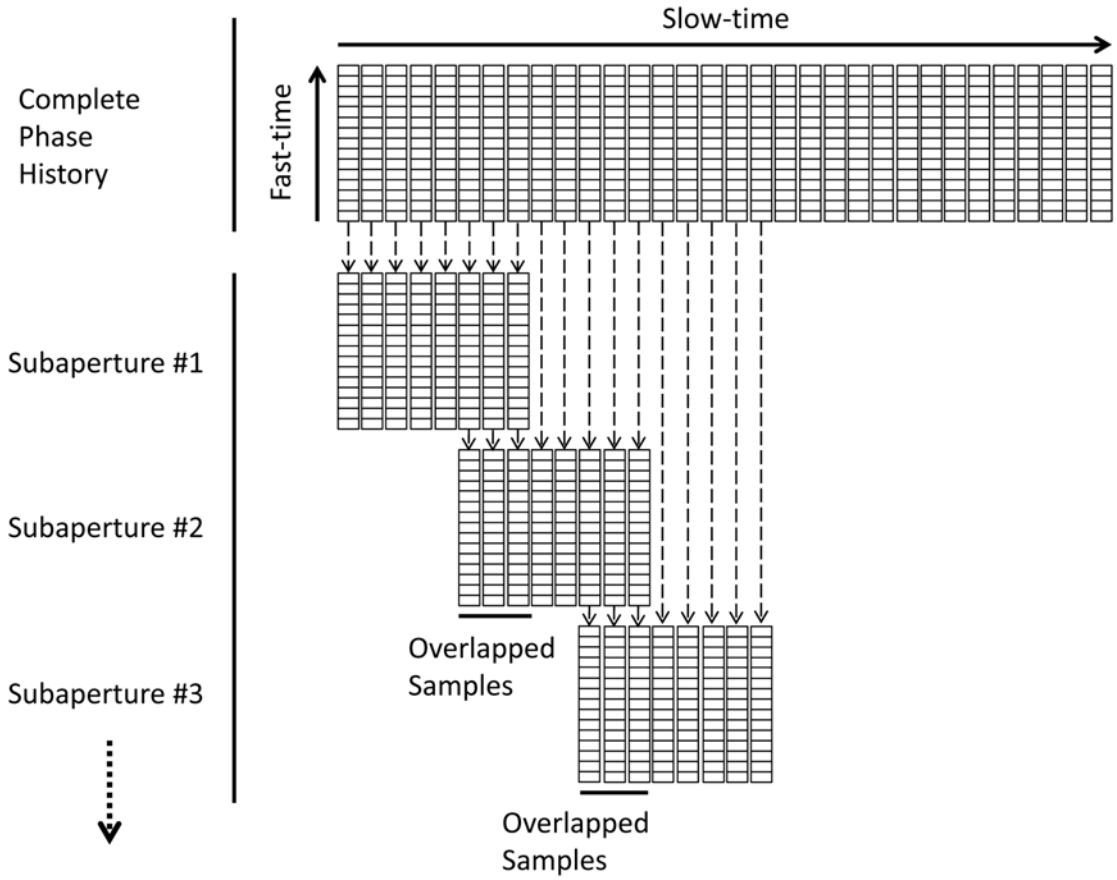

Figure 4.4: Subaperture Division

A subaperture of the phase history once the FFT is applied is a coarse resolution image for a small region of the image. With the coarse resolution image, since the location of the subaperture itself is known and scatterers within the image are resolved (even at a coarse resolution), phase corrections for the residual range error can be applied; this is done at each level of subaperture processing [12]. Within each level of subaperture processing, resolution improves and errors are corrected [12].

Using tiers of subapertures, Doerry is able to go beyond the scene diameter limit set by Walker as (setting $\phi_{qpe,\max} = \frac{\pi}{2}$) [1]

$$D \le 4\rho\sqrt{\frac{|r_{c,0}|}{\lambda_0}} \tag{4.12}$$

to the following limit [12]

$$D \le 4\rho\left(\frac{|r_{c,0}|}{\lambda_0}\right)^{\frac{N_s+1}{N_s+2}} \tag{4.13}$$

where

N_s is the number of levels or tiers of subapertures

Doerry's dissertation [13] provides further details on the tier processing technique and its scene size limit expression.

4.4 Dual Format Algorithm

The Dual Format Algorithm (DFA) is not a correction to typical PFA processing; it processes data in a different, novel order. DFA is included in this report because it corrects for the residual range phase error that is a result of PFA while processing data on a polar grid; the method by which this is done is fairly unique. Typically for PFA processing data is interpolated from a polar grid to a rectangular grid, then the FFT is applied. DFA applies the FFT on the data first, then resamples the data to a rectangular grid for display [14].

An advantage to DFA over previous methods, such as Doren [7] and Doerry [6], comes from the expression for the differential range in polar coordinates. It turns out that in polar coordinates, the quadratic phase error is only a function of range and independent of azimuth position. The range is well known and the correction can be efficiently applied across all slow-time samples after the range FFT is applied. In comparison to other methods [6, 7, 8, 9, 10, 14] correcting quadratic wavefront curvature have had an image domain x and y dependence and/or needed the flight geometry to estimate the location of frequency domain data to apply a correction after the image is formed.

Another advantage for DFA comes from the efficiency that can be gained from a single interpolation within the image formation process. Typical PFA requires a geometric distortion

correction (section 4.1) to remove linear phase errors; this is an image domain resampling. DFA combines the geometric distortion correction with the polar to rectangular interpolation into one interpolation operation [14].

5 Summary

This report has presented a development of the Polar Format Algorithm (PFA) to illustrate the location and type of assumptions and approximations that are embedded; they are ignoring residual video phase, flattening target scene height, and assuming planer wavefronts. Residual video phase can be completely corrected [2, 6], and is not a consequence of PFA. The image effects from setting scene height to zero were discussed in chapter 3; these image effects can be either ignored or exploited. While corrections for geometric distortions are straight-forward resample operation [2], correcting the quadratic and higher order distortions are not as straight-forward to correct because they depend on the location of the scatterer. Furthermore, Section 2.3 shows how the planer wavefront approximation is necessary to apply the Fourier transform to resolve scatterer location. Chapter 4 showed three distinct methods and several variations thereof to mitigate the quadratic and higher order errors.

Radar designers will always be balancing performance trade-offs for their particular system and application. It should not be expected that any one method can be 'taken off the shelf' and applied to their system; inevitably there are changes that must be made to apply the algorithm and changes can be made to improve the algorithm. With improvements in digital signal processing technology and variations in radar hardware over time, the subject of wavefront curvature correction will remain an active research area.

5.1 Future Work

5.1.1 Determining Residual Phase Error

While Walker and others have used dominant terms in the Taylor series expansion of the differential range phase expression to bound the application of corrections, it is really the difference between the true differential range and the approximate value of the differential range. Instead of an analytical bound of one or two terms, one could study the phase from the true differential range phase value and compare it to the corrections that are available to determine if the residual phase error is within tolerable limits. This method could be particularly useful in the case of modeling total phase error budget for a system, and the radar designer needs to know at what point the residual terms contribute non-negligible distortions into image products. For a radar designer, there are many reasons to want to quantify the phase error throughout an entire

radar system. Many components of a practical synthetic aperture radar system contribute to the total phase error. Quantifying the contributions from image formation can help develop a phase error margin for the entire system.

5.1.2 Taylor Series Expansion Point and Chip Selection

The Taylor series expansion approximates a function at a specific point, or function value. Taylor series terms most accurately describe the function near the expansion point. This expansion point could be moved to other locations. Some techniques use the center of the image while others use a chip (or subimage) to center the Taylor series expansion. There could be a lot more study devoted to selecting optimal chip size, shape, and location. For instance, little correction is needed near the scene center, so determine how far from scene center has an acceptable level of error and do not apply corrections within that region. Further study could look at selecting a chip shape and location based on the correction being applied. An azimuth correction could be applied in chips divided only in the azimuth dimension. There are many questions to be answered for selecting chips in an image, these include:

- Is there a more efficient or accurate (or both) place to center the chip?
- Do image chips need to all be the same size?
- Is there a particular dimension of the image chip that is more sensitive to phase errors?
- Do image chips need to be resized and relocated based on the phase correction?
- Do all image chips need the same number of corrections?
- Perhaps only certain chips need particular corrections.
- Do chips need to be rectangular in shape, is there a benefit from overlapping chips?

5.1.3 Iterative Correction

An analytical model can be developed for the image based on radar parameters and the size of the scene to estimate the differential range phase that should be expected from a particular location within the image. Use this analytical model to iteratively apply phase error corrections to the image to only the region of the image where it is needed until the analytical model has a reasonable amount of residual phase error. For example, first a geometric correction is made, then, a quadratic modification could be applied to regions of the image where it is needed.

References

[1] Walker, Jack L., “Range-Doppler Imaging of Rotating Objects,” *IEEE Transactions on Aerospace and Electronic Systems*, Vol. AES-16, No. 1, Jan 1980.

[2] Carrera, Walter G., Goodman, Ron S., Majewski, Ronald M., *Spotlight Synthetic Aperture Radar: Signal Processing Algorithms*, Artech House, 1995.

[3] Jakowatz, Charles V., Wahl, Daniel E., Eichel, Paul H., Ghiglia, Dennis C., Thompson, Paul A., *Spotlight-Mode Synthetic Aperture Radar: A Signal Processing Approach*, Springer, 1996.

[4] Martin, Grant D., Doerry, Armin W., “SAR Polar Format Implementation with MATLAB,” Sandia National Laboratories report SAND2005-7413, Unlimited Release.

[5] Doerry, Armin W., “Basics of Polar-Format Algorithm for Processing Synthetic Aperture Radar Images,” Sandia National Laboratories report SAND2012-3369, Unlimited Release.

[6] Doerry, Armin W., “Wavefront Curvature Limitations and Compensation to Polar Format Processing for Synthetic Aperture Radar Images,” Sandia National Laboratories report SAND2007-0046, Unlimited Release.

[7] Doren, Neall E., “Space-Variant Post-Filtering for Wavefront Curvature Correction in Polar-Formatted Spotlight-Mode SAR Imagery,” Sandia National Laboratories Report SAND99-2706, Unlimited Release, 1999.

[8] Linnehan, Robert, Yasuda, Mark, Doerry, Armin, “An Efficient Means to Mitigate Wavefront Curvature Effects in Polar Format Processed SAR Imagery,” *Radar Sensor Technology XVI*, Proc. of SPIE Vol. 8361, 2012.

[9] Garber, Wendy L., Hawley, Robert W., “Extensions to Polar Formatting with Spatially Variant Post-Filtering,” *Algorithms for Synthetic Aperture Radar Imagery*, Proc. of SPIE Vol. 8051, 2011.

[10] Mao, Xinhua, Zhu, Daiyin, Zhu, Zhaoda, “Polar Format Algorithm Wavefront Curvature Compensation Under Arbitrary Radar Flight Path,” *IEEE Geoscience and Remote Sensing Letters*, Vol. 9, No. 3, May 2012.

[11] Burns, B. L., Cordaro, J. T., “A SAR Image-Formation Algorithm that Compensates for the Spatially-Variant Effects of Antenna Motion,” *Algorithms for Synthetic Aperture Radar Imagery*, Proc. of SPIE Vol. 2230, 1994.

[12] Doerry, Armin W., “Synthetic Aperture Radar Processing with Polar Formatted Subapertures,”, *1994 Conference Record of the Twenty-Eighth Asilomar Conference on Signals, Systems and Computers*, Vol. 2, pg 1210-1215.

[13] Doerry, Armin W., “Synthetic Aperture Radar Processing with Tiered Subapertures,” Sandia National Laboratories Report SAND94-1390, Unlimited Release, 1994.

[14] Gorham, LeRoy A., Rigling, Brian D., “Dual Format Algorithm for Monostatic SAR,” *Algorithms for Synthetic Aperture Radar Imagery XVII*, Proc. of SPIE Vol. 7699, 2010.

[15] Liu, Q., Hong, W., Tan, W.-X., Lin, Y., Wang, Y.-P., Wu, Y.-R., “An Improved Polar Format Algorithm with Performance Analysis for Geosynchronous Circular SAR 2D Imaging,” *Progress in Electromagnetics Research*, Vol. 119, 155-170, 2011.

[16] Preiss, M., Gray, D., Stacy, N., “Space Variant Filtering of Polar Format Spotlight SAR Images for Wavefront Curvature Correction and Interferometric Processing,” *2002 IEEE International Geoscience and Remote Sensing Symposium*, Vol. 1, 2002.

[17] Wang, X., Zhu, D., Mao, X., Zhu, Z., “Space-Variant Filtering for Wavefront Curvature Correction in Polar Formatted Bistatic SAR Image,” *IEEE Transactions on Aerospace and Electronic Systems*, Vol. 48, No. 2, 2012.

[18] Wang, X., Zhu, D., “Wavefront Curvature Correction in One Stationary Bistatic SAR Image Focused Via PFA,” *Electronics Letters*, Vol. 46, Issue 18, pg1291-1293, 2010.

Distribution

4 Oklahoma State University (electronic copy)
Attn: James West, Charles Bunting, Daqing Piao, George Scheets
202 Engineering South
Stillwater, OK 74078

1	MS0532	James Hudgens	5340 (electronic copy)
1	MS0532	Bryan Burns	5340 (electronic copy)
1	MS0533	Tim Bielek	5342 (electronic copy)
1	MS0533	David Harmony	5342 (electronic copy)
1	MS0533	Robert Riley	5342 (electronic copy)
1	MS0533	Bobby Rush	5342 (electronic copy)
1	MS0532	William H. Hensley	5344 (electronic copy)
1	MS0519	Doug Bickel	5344 (electronic copy)
1	MS0519	Ernest Gentry	5344 (electronic copy)
1	MS0532	Cameron Musgrove	5344 (electronic copy)
1	MS0519	Rick Naething	5344 (electronic copy)
1	MS0519	Ann Raynal	5344 (electronic copy)
1	MS0519	Armin Doerry	5349 (electronic copy)


Sandia National Laboratories